Pergamon

Int. J. Heat Mass Transfer. Vol. 40, No. 9, pp. 2147–2164, 1997

0017–9310/97 $17.00+0.00

PII: S0017-9310(96)00269-4

Flooding limit in closed, two-phase flow thermosyphons

MOHAMED S. EL-GENK and HAMED H. SABER†

Institute for Space and Nuclear Power Studies, Department of Chemical and Nuclear Engineering, University of New Mexico, Albuqerque, NM 87131-1341, U.S.A.

(*Received* 26 *April* 1996 *and in final form* 11 *July* 1996)

Abstract—A one-dimensional, steady-state analytical model was developed to predict the CCFL in GATPTs, which treats the shear stress at the liquid–vapor interface as the sum of two terms: (a) adiabatic shear stress; and (b) dynamic shear stress. The latter accounts for the effect of evaporation/condensation at the liquid–vapor interface. The model predictions were in good agreement (within ±10%) with the data of other investigators for water and methanol. The results showed that neglecting the dynamic shear stress at intermediate and high liquid film flows underestimates the film Reynolds number at CCFL by more than 20%. The model was used to develop operation maps for R-113, acetone, methanol, heptane, water and Dowtherm-A working fluids, which give the film Reynolds number at the CCFL (or maximum power throughput) as a function of the vapor temperature in the range from 250 to 700 K. The effects of the thermosyphon inner diameter and length of the evaporator section on the film Reynolds number at CCFL were also investigated.

INTRODUCTION

Closed, gravity assisted, two-phase thermosyphons (GATPTs) are widely being used in many energy and industrial applications. Examples include gas–gas and liquid–gas heat exchangers; recovery of low grade heat in chemical and electric power plants; pollution and emission control in smoke stack industries; collection and utilization of solar energy; domestic heating and cooling; thawing of snow on major roads; thermal control of food storage units and commercial fisheries; food drying; and thermal treatment of exterior coating in auto industries. The GATPT design is relatively simple; it is basically a wickless heat pipe which utilizes the evaporation and condensation of the working fluid to transport heat at high rates (Fig. 1). The evaporator and condenser, located at the lower and upper ends of the thermosyphon, respectively, are separated by an adiabatic section, whose length depends on the distance between the heat source and heat sink. The evaporator is partially filled with a working fluid, which is degassed and kept initially at a slight vacuum. The working fluid in the evaporator section absorbs the heat input in the form of sensible heat and mostly as latent heat of vaporization. The vapor travels upward to the condenser section where it is converted into liquid, giving up its latent heat of condensation. The liquid then flows downward on the wall as a thin film under the effect of gravity to the evaporator section.

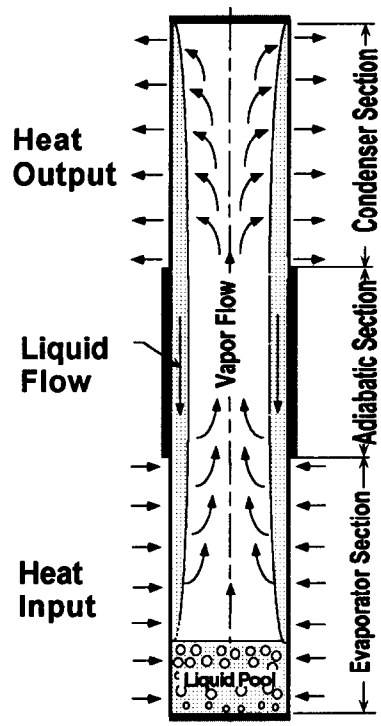

Fig. 1. A schematic of a closed GATPT.

At low and intermediate power inputs, the vapor flow rate and, hence, the rate of liquid return to the evaporator as well as the thickness of the liquid film in the adiabatic-section increase as the input power increases. At a high input power, however, the liquid–vapor (L–V) interface near the exit of the evaporator,

† Visiting Research Engineer and Ph.D. candidate in the Faculty of Engineering, Mansoura University, Arab Republic of Egypt.

NOMENCLATURE

A	vapor flow area [m^2]
A_1–A_4	coefficients, eqn (23)
A_5	coefficient, eqn (28)
A_6, A_7	coefficients, eqn (32)
Bo	Bond number based on d_i, $d_i(\sigma_l/((\rho_l-\rho_v)g))^{-0.5}$
B_1–B_3	coefficients, eqn (23)
Bo_δ	Bond number based on δ, $\delta(\sigma_l/((\rho_l-\rho_v)g))^{-0.5}$
C_1, C_2	coefficients, eqn (16)
C_3, C_4	coefficients, eqn (23)
d	diameter [m]
f	friction factor
g	gravitational acceleration [m^2 s^{-1}]
Gr	two-phase Grashof number, $(8gR_i^3/v_l^2)^{0.5}$
G_1–G_4	coefficients, eqn (13)
h_{fg}	latent heat of vaporization [J kg^{-1}]
K	modified Kutateladze number, eqn (2)
L	length [m]
Q	power input, power throughput [W]
Q^*	power throughput at onset of flooding [W]
R	radius [m]
Re_f	film Reynolds number, $(4W_l/\mu_l)$
Re_f^*	film Reynolds number at onset of flooding
T	temperature [K]
u	flow velocity [m s^{-1}]
W	mass flow rate per unit perimeter [kg m·s^{-1}]
X_1–X_3	coefficients, eqn (23)
x	axial coordinate, thickness [m]
y	radial coordinate.

Greek symbols

β_1	coefficient, eqn (29)
β_2, β_3	coefficients, eqn (32)
δ	liquid film thickness in adiabatic section [m]
δ^*	liquid film thickness in adiabatic section at CCFL [m]
Δ	dimensionless liquid film thickness in adiabatic section, (δ/R_i)
μ	dynamic viscosity [N·s m^{-2}]
v	kinematic viscosity [m^2 s^{-1}]
ρ	density [kg m^{-3}]
σ	surface tension [N m^{-1}]
τ	shear stress [N m^{-2}]
τ^*	shear stress at CCFL [N m^{-2}].

Subscripts

a	adiabatic section
c	condenser section
d	dynamic
e	evaporator section
f	liquid film
i	L–V interface, inner tube surface
ia	interfacial adiabatic
id	interfacial dynamic
it	interfacial total for turbulent film
l	liquid
L	laminar
R	reference
sw	wall outer surface
sat	saturation
t	turbulent
v	vapor
w	inner tube surface, L–W interface
wL	wall-laminar film interface
wt	wall-turbulent film interface.

Superscripts

–	average.

where vapor flow is highest, becomes agitated and wavy, decreasing the rate of liquid return to the evaporator, at the expense of increasing the thickness of the liquid film. A mismatch between the rate of liquid return to the evaporator and the heat input could eventually cause a dryout of the liquid film in the evaporator section. The "onset of flooding" or CCFL at the exit of the evaporator is the focus of this paper.

As will be shown later in the model development and results sections, the dynamic component of the interfacial shear stress due to evaporation/condensation in a thermosyphon is added to the adiabatic shear stress component in the condenser, but subtracted from it in the evaporator section. As a result of the higher total interfacial shear stress in the condenser section, the CCFL occurs first at the exit of the condenser (adjacent to the adiabatic section), which has been confirmed by many visualization experiments (for example, [1]). Although liquid flooding at the exit of the evaporator section occurs at a somewhat higher film Reynolds number, or power throughput, than at the exit of the condenser, it directly influences the liquid film dryout in the evaporator. Therefore, the emphasis in this paper is on the condition affecting the CCFL at the exit of the evaporator because of its impact on the potential dryout of the liquid film in the evaporator due to insufficient liquid return. In addition to this type of liquid film dryout, Shiraishi *et al.* [1] in their flow visualization experiments have identified another type of dryout, referred to as liquid pool/film dryout. This film dryout is associated with inadequate working

fluid inventory (or fill ratio) in the evaporator section of a thermosyphon.

Bharathan *et al.* [2] have shown that at a low liquid film Reynolds number, the shear stress at the liquid–vapor (L–V) interface is negligible and the liquid film flow can be accurately predicted by the Nusselt solution. At intermediate and high liquid film Reynolds numbers, however, the shear stress at the L–V interface becomes progressively important, retarding the liquid film flow to the evaporator. Hence, in order to accurately predict the CCFL in GATPTs, it is important to incorporate the actual shear stress at L–V interface, including the dynamic effect due to evaporation/condensation. Several empirical correlations for predicting CCFL in GATPTs have been reported, for example [3–7]. The recent correlation of Faghri *et al.* [8], which is a combination of those of Tien and Chung [4] and of Imura *et al.* [6], has demonstrated the best agreement with the experimental data for different working fluids; it gives the maximum power throughput at the onset of flooding as:

$$Q^* = Kh_{fg}A(g\sigma(\rho_l-\rho_v))^{0.25}(\rho_l^{-0.25}-\rho_v^{-0.25})^{-2}, \tag{1}$$

where

$$K=(\rho_l/\rho_v)^{0.14}\tanh^2 Bo^{0.25}. \tag{2}$$

Equation (1) incorporates the effect of the thermosyphon inner diameter in the Bond number, Bo, and in the vapor flow area, A, but neglects the effect of liquid viscosity.

Analytical models have also been reported for predicting CCFL, for example [9–12]. In a recent review, Peterson and Bage [13] indicated that the predictions of CCFL by the different models available at the time of their review, except that of Reed and Tien [10], varied by as much as a factor of five. The model of Reed and Tien [10] and the most recent ones of Zuo and Gunnerson [11] and Roesler and Groll [12] each calculated the shear stress at the L–V interface by arbitrarily modifying the adiabatic interfacial friction coefficient correlations and neglecting the dynamic effect due to evaporation/condensation. The proposed modifications improved the comparison of the models with the experimental data, by lowering the actual shear stress at the L–V interface at the exit of the evaporator, at intermediate and high liquid film Reynolds numbers.

Reed and Tien [10] evaluated the L–V interfacial shear stress based on the average velocity of the liquid film, rather than the velocity of the interface, and effectively changed the first constant on the right-hand-side of equation (18) from -0.56 to -0.59. Also, in order to account for the fact that the average shear stress at the L–V interface may differ from the product of the modified adiabatic interfacial friction coefficient and the average dynamic pressure, they introduced two weighting factors for laminar and turbulent films, respectively, assuming that: (a) the liquid film flow in the condenser can be given by Nusselt solution; (b) the liquid film flow thickness and flow rate in the adiabatic section are constant; and (c) the liquid film flow in the evaporator varies linearly down the wall and the film thickness is constant, for an isoflux heat input.

Recently, Roesler and Groll [12] performed flow field visualization experiments in an annular thermosyphon and developed an analytical model for predicting CCFL for laminar film flow. Their model modified the adiabatic friction factor correlation of Bharathan *et al.* [2] (equation 18) to read:

$$\log_{10}(A) = -0.269+9.85/Bo, \tag{3}$$

which gives a smaller friction coefficient at L–V interface than Bharathan *et al.* original correlation (equation 17). They also modified Grolmes *et al.* correlation for the adiabatic friction coefficient [14] by substituting a smaller value of 8.1×10^5 m^{-2} (instead of 2×10^6 m^{-2}) for the constant "A" in the second term on the right-hand-side of equation (19). The predictions of Roeslor and Groll's model agreed with their own data for water to within $\pm20\%$.

Both Reed and Tien [10] and Roesler and Groll [12] also neglected the liquid film thickness when determining the vapor flow area at CCFL. Since the liquid film thickness in the adiabatic section could be as much as 0.2 mm or more [12], neglecting the film thickness overestimates the vapor flow area by more than 8.5 and 4% for a GATPT having an inner diameter of 10 and 20 mm, respectively; hence overpredicting the maximum power throughput at CCFL, which is directly proportional to the flow area of vapor (equation 1).

Zuo and Gunnerson [11] have developed a one-dimensional, steady-state model for predicting the CCFL at the exit of the evaporator. Their liquid film momentum conservation equation incorporated an advection term, but defined the shear stress at the wall based on the average film flow velocity, rather than the velocity gradient at the wall. They incorporated the modified Bharathan *et al.* correlation for the interfacial friction coefficient used by Reed and Tien [10] and evaluated the interfacial shear stress on the bases of the average film velocity, instead of the L–V interfacial velocity. The model predictions of the film Reynolds number at CCFL agreed reasonably well with the water data of Prenger [7] and the author's own data. In summary, analytical models for CCFL have neglected the dynamic shear stress at the L–V interface. Instead, they modified the adiabatic interfacial friction coefficient correlations in such a way to improve the comparison with experimental data. The proposed modifications reduced the interfacial shear stress at the exit of the evaporator, which partially compensated for neglecting the dynamic shear stress due to evaporation

The objective of this work is to develop an analytical model to predict the CCFL in GATPTs at the exit of

the evaporator on the bases of incorporating the shear stress at the L–V interface as the sum of two terms: (a) adiabatic shear stress, based on original correlations of Bharathan *et al.* [2] and Grolmes *et al.* [14]; and (b) dynamic shear stress, to account for the effect of evaporation at the L–V interface [15, 16]. A parametric analysis was performed to quantify the effects of the vapor temperature and evaporator length on the liquid film thickness and Reynolds number corresponding to the CCFL for water at the exit of the condenser and the evaporator, respectively. The model predictions were compared with experimental data of other investigators for water and methanol to quantify the effect of the dynamic shear stress on liquid film thickness and Reynolds number at CCFL at the exit of the evaporator. The effects of thermosyphon inner diameter and evaporator length on CCFL were also investigated. In addition, operation maps for R-113, acetone, methanol, heptane, water and Downtherm-A working fluids were developed for vapor temperature from 250 to 700 K.

ANALYTICAL MODEL

The present model is comprised of two separate flow models: laminar and turbulent liquid film flow models. Because the transition regime is not well defined, several values have been suggested for the film Reynolds number for transition to turbulent flow, which ranged from 1200 to 2400 [3, 17]. Reed and Tien [10] and Zuo and Gunnerson [11], however, assumed the transition flow regime to extend from a film Reynolds number of 2040–3500. In this paper, the transition regime is assumed to occur for liquid film Reynolds number from 1200 and 3500. In this regime, the liquid film Reynolds numbers at the CCFL were determined by interpolating the values of laminar ($Re_f \leqslant 1200$) and turbulent ($Re_f \geqslant 3500$) film flows. The liquid–wall (L–W) and L–V interfaces were treated as a non-slip and a slip boundary, respectively (Fig. 2). The heating and cooling heat fluxes in the evaporator and condenser were uniform. The model incorporates the following assumptions: (a) saturation vapor temperature in the adiabatic section equals that of the L–V interface at the exit of evaporator; (b) effect of vapor compressibility is negligible, which is justified in countercurrent two-phase systems [3, 17]; (c) heat transfer through liquid film is solely by conduction, owing to its small thickness; (d) axial pressure drop in the film is negligible; (e) effect of liquid droplets entrainment in vapor flow is negligible, which is justified except near CCFL; (f) momentum advection in liquid film is negligible, since its thickness in adiabatic section is almost uniform; and (g) average vapor flow velocity is equal to that at the L–V interface.

Laminar liquid film flow model

The solution of the momentum balance equation for laminar flow film,

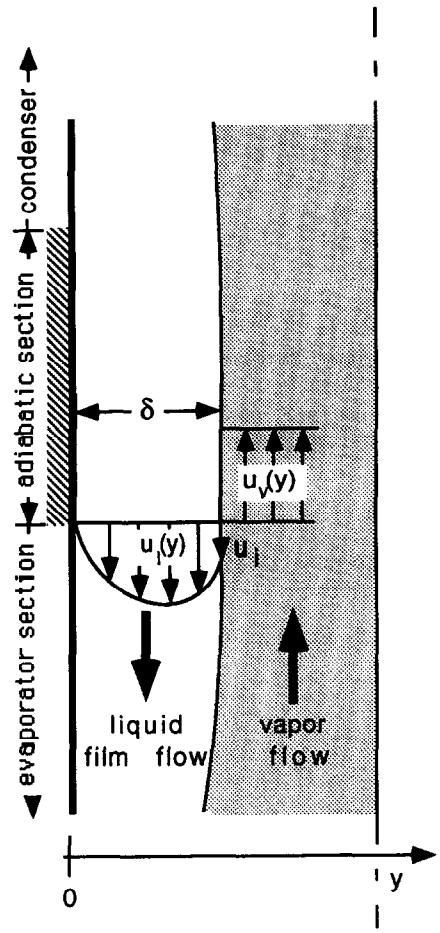

Fig. 2. Liquid and vapor flow model for a GATPT.

$$\mu_l\left(\frac{\partial^2 u_l}{\partial y^2}\right)+(\rho_l-\rho_v)g=0, \tag{4}$$

subject to the boundary conditions:

$$u_l=0 \quad \text{at } y=0, \tag{5a}$$

and

$$\mu_l\left(\frac{\partial u_l}{\partial y}\right)=-\tau_i \quad \text{at } y=\delta, \tag{5b}$$

yields the following expression for the radial distribution of the liquid flow velocity:

$$u_l(y)=\left(\frac{(\rho_l-\rho_v)g\delta-\tau_i}{\mu_l}\right)y-\left(\frac{(\rho_l-\rho_v)g}{2\mu_l}\right)y^2, \tag{6}$$

which upon integration gives the average flow velocity in the liquid film as:

$$\bar{u}_l=\left(\frac{(\rho_l-\rho_v)g}{3\mu_l}\right)\delta^2-\left(\frac{\tau_i}{2\mu_l}\right)\delta. \tag{7}$$

The shear stress at the L–V interface, τ_i, can generally be expressed as [15]:

$$\tau_i = \tau_{ia} \pm \tau_{id} = \tau_{ia} \pm (u_i + u_v)\frac{dW_v}{dx}, \quad (8)$$

where the plus and minus signs of the second term on the right-hand-side of equation (8) account for the effect of condensation and evaporation at the L–V interface, respectively. Equation (8) can be written in terms of the power throughput, Q, as:

$$\tau_i = \tau_{ia} \pm (u_v + u_i)(Q/(\pi d_i L_e h_{fg})). \quad (9)$$

Equations (8) and (9) indicate that the dynamic shear stress reduces the total shear stress at L–V interface in the evaporator and increases it in the condenser, hence, increasing and decreasing the film Reynolds number at the onset of flooding at the exit of the evaporator and the condenser, respectively, beyond its adiabatic value. The average vapor velocity at the evaporator exit is:

$$u_v = Q/(0.25\pi(d_i - 2\delta)^2 \rho_v h_{fg}), \quad (10)$$

and the corresponding L–V interfacial velocity from equation (6) is:

$$u_i = \left(\frac{(\rho_l - \rho_v)g\delta - \tau_i}{\mu_l}\right)\delta - \left(\frac{(\rho_l - \rho_v)g}{2\mu_l}\right)\delta^2. \quad (11)$$

Substituting for u_v and u_i into equation (9) gives:

$$\tau_i(1 \pm G_4) = \tau_{ia} \pm G_1(G_2 + G_3), \quad (12)$$

where

$$G_1 = Q(\pi d_i L_e h_{fg})^{-1} = 0.25 Re_f(\mu_l/L_e),$$

$$G_2 = (\rho_l - \rho_v)g\delta^2/2\mu_l = ((\rho_l - \rho_v)/\rho_l)(\nu_l/16R_i)\Delta^2 Gr_f^2,$$

$$G_3 = Q(0.25\pi(d_i - 2\delta)^2 \rho_v h_{fg})^{-1} = Re_f(\nu_l/d_i)(\rho_l/\rho_v)/(1-\Delta)^2$$

and

$$G_4 = Q\delta(\pi d_i L_e \mu_l h_{fg})^{-1} = 0.25 Re_f \Delta(R_i/L_e). \quad (13)$$

For calculating the CCFL at the exit of the condenser section, the second term on the right-hand-side of equation (12) has a positive sign and L_e on the right-hand-side of equations (9) and (13) is replaced with L_c. When $Q = 0$, the interfacial shear stress equals the adiabatic shear stress:

$$\tau_{ia} = 0.5 f_{ia} \rho_v (u_v + u_{ia})^2. \quad (14)$$

Substituting for u_v and u_{ia} into equation (14) gives the adiabatic shear stress as:

$$\tau_{ia} = C_1(2 + C_2(G_2 + G_3) + 2.0\sqrt{1 + C_2(G_2 + G_3)}), \quad (15)$$

where

$$C_1 = (\mu_l^2/(2 f_{ia} \rho_v \delta^2)) \quad \text{and} \quad C_2 = \mu_l/(\delta C_1). \quad (16)$$

The adiabatic friction coefficient in equation (16) is evaluated using one of the following correlations:

(a) Bharathan *et al.* [2]

$$f_{ia} = 0.005 + A Bo_\delta^b, \quad (17)$$

where

$$\log_{10} A = -0.56 + 9.07 Bo^{-1}$$

$$\text{and} \quad b = 1.63 + 4.74\, Bo^{-1}. \quad (18)$$

(b) Grolmes *et al.* [14]:

$$f_{ia} = 0.006 + A\delta^2(\mu_l/\mu_R)^{-0.44}, \quad (19)$$

where $A = 2 \times 10^6$ (m^{-2}) and μ_R is a reference liquid viscosity = 1.0 CP. For a laminar liquid film flow, the wall interfacial shear stress, assuming a non-slip condition at the wall, is expressed as:

$$\tau_w = (\rho_l - \rho_v)g\delta[(1/3) + 4(\rho_l/(\rho_l - \rho_v))(Re_f / Gr_f^2 \Delta^3(1 - 0.5\Delta))]. \quad (20)$$

This equation is the same as in Reed and Tien's [10] and Roesler and Groll's [12], but differs from that of Zuo and Gunnerson [11], who expressed the wall shear stress in terms of the average liquid velocity in the film (equation 7). Consequently, the wall shear stress for a laminar flow in Zuo and Gunnerson's model was lower than that given by equation (20) by the amount $((\rho_l - \rho_v)g\delta/3)$. In their model, since the shear stress at the liquid–vapor interface was the same as in Reed and Tien's, but the shear stress at the wall was lower, the calculated film Reynolds number at the onset of flooding would be higher. On the other hand, neglecting the dynamic shear stress at the liquid–vapor interface in both models lowers the film Reynolds number at CCFL. These competing effects are quantified later in the results section.

The steady-state mass conservation equations in the liquid film at the exit of the evaporator section gives another relation for the average film flow velocity:

$$\bar{u}_l = (Q/(\pi(d_i - \delta)\delta h_{fg} \rho_l)). \quad (21)$$

Equating equations (7) and (21) and rearranging the results gives the steady-state power throughput as:

$$Q = (X_1 + \sqrt{X_1^2 - 4X_2^2(X_3^2 - C_3)})/(2X_2^2), \quad (22)$$

where

$$X_1 = 2X_2X_3 - C_4, \quad X_3 = 2B_1 + B_2 - (A_1/A_2),$$

$$X_2 = -(A_4B_3 + (A_3/A_2)), \quad C_3 = 4B_1(B_1 + B_2),$$

$$C_4 = -(4A_4B_1B_3), \quad A_1 = (\rho_l - \rho_v)g\delta^2/(3\mu_l),$$

$$A_2 = f_{ie}\rho_v\delta/(4\mu_l), \quad A_3 = [\pi(d_i - \delta)\delta h_{fg}\rho_l]^{-1},$$

$$A_4 = [0.25\pi(d_i - 2\delta)^2 h_{fg}\rho_v]^{-1},$$

$$B_1 = \mu_l^2/(\rho_v\delta f_{ie})^2, \quad B_2 = (\rho_l - \rho_v)g\delta/(\rho_v f_{ie}),$$

$$B_3 = 2.0\sqrt{B_1} \quad \text{and} \quad f_{ie} = 2\tau_i/(\rho_v(u_v+u_i)^2). \quad (23)$$

Turbulent liquid film flow model

The force balance in the liquid film at the exit of the evaporator section yields:

$$\tau_{wt}+\tau_{it} = (\rho_l-\rho_v)g\delta. \quad (24)$$

However, since the liquid velocity at the L–V interface is not readily available, the shear stresses at the wall and the L–V interfaces may be expressed in terms of the average film flow velocity (equation 21), after accounting for the fact that they may deviate from the product of the interfacial friction coefficient and the average dynamic pressure in the film. Thus, the interfacial shear stress at the wall for the turbulent film may be given as:

$$\tau_{wt} = (f_{wt}/f_{wL})(2\mu_l W_l/\rho_l\delta^2), \quad (25)$$

where $f_{wL} = 16/Re_f$ and the wall friction coefficient, f_{wt}, is given by the Blasius relation:

$$f_{wt} = 0.079Re_f^{-0.25}. \quad (26)$$

The shear stress at the wall can also be expressed in terms of the input power to evaporator as

$$\tau_{wt} = A_5 Q^{7/4}, \quad (27)$$

where

$$A_5 = 0.02793\rho_l\beta_l A_3^2[\pi d_i h_{fg}\mu_l]^{0.25}, \quad (28)$$

$$\beta_l = ((d_i-\delta)/d). \quad (29)$$

Also, the shear stress at the L–V interface for the turbulent film flow can generally be expressed as:

$$\tau_{it} = \beta_2\tau_{ia} \pm \beta_3\tau_{id}, \quad (30)$$

where the plus and minus signs of the second term on the right hand side of equation (30) account for the effect of condensation and evaporation at L–V interface, respectively. In terms of the power throughput corresponding to CCFL, equation (30) can be written as:

$$\tau_{it} = (A_7 \pm A_6)Q^2, \quad (31)$$

where

$$A_6 = ((A_3+A_4)\beta_3/(\pi d_i h_{fg}L_c)),$$

$$A_7 = 0.5f_{ia}\rho_v\beta_3^2(A_3+A_4)^2, \beta_2 = \beta_3^2 \quad \text{and}$$

$$\beta_3 = (2A_3+A_4-(A_1/2Q))/(A_3+A_4). \quad (32)$$

The coefficients β_2 and β_3 account for the deviation of the interfacial shear stress for the turbulent film flow from the product of the interfacial friction coefficient and the dynamic pressure in the film. These coefficients were evaluated from equating the shear stresses for the laminar and the turbulent film flows at the wall-film and the L–V interfaces. For calculating the CCFL at the exit of the condenser section, the second term on the right-hand-side of equation (31) has a positive sign and L_e on the right-hand-side of equation (32) is replaced with L_c.

Substituting for the wall shear stress and liquid–vapor interfacial shear stress from equations (27) and (31) into equation (24) gives the steady-state power throughput for the turbulent film flow as:

$$A_5 Q^{7/4} + (A_7 \pm A_6)Q^2 = (\rho_l-\rho_v)\delta g. \quad (33)$$

Equations (22) and (33) are solved iteratively for both Q^* and corresponding film thickness. When concerned with CCFL at the exit of the condenser use the plus sign for the coefficient A_6 in equation (33). The solution evaluated the wall thermal conductivity at the wall temperature; the properties of the vapor at its saturation temperature at the exit of the evaporator, T_v, and those of the liquid film at the average film temperature $((T_v+T_w)/2)$. The vapor temperature, T_v, can be expressed as:

$$T_v = T_{sw} - Q((x_w/(A_w k_w)) + (\delta/(A_\delta k_l))), \quad (34)$$

where

$$A_w = 2\pi x_w L_e/\ln((d_i+x_w)/d_i) \quad \text{and}$$

$$A_\delta = 2\pi\delta L_e/\ln(d_i/(d_i-2\delta)). \quad (35)$$

Neglecting the flow area of the liquid film when evaluating its thermal resistance also introduces an error in calculating the vapor temperature and, hence, in the value of Reynolds number at CCFL.

RESULTS AND DISCUSSION

The model predictions of the total interfacial shear stress and the liquid film Reynolds number and thickness corresponding to the CCFL at the exit of both the condenser and the evaporator sections of a water thermosyphon are compared in Fig. 3. As indicated by equations (12) and (30) for laminar and turbulent liquid film flow, respectively, vapor condensation increases the total shear stress at the exit of the condenser, while liquid evaporation reduces the total interfacial shear stress at the exit of the evaporator (Fig. 3a). Consequently, the CCFL is reached first at the exit of the condenser, at a lower liquid film Reynolds number, but a higher liquid film thickness (Fig. 3b, c). For a condenser and evaporator sections which are 1.2 m long each, and a vapor temperature of 360 K, the CCFL at the exit of the condenser occurred at a dimensionless liquid film thickness of 0.0299 and Reynolds number of 164, compared to 0.0274 and 196, respectively, at exit of evaporator. These differences in the values of the liquid film thickness and Reynolds number are because for the same evaporator and condenser length, the total interfacial shear stress at the exit of the former was smaller than the latter. For example, at a water vapor temperature of 360 K, the adiabatic interfacial shear stress, τ_{ia}, was about 0.71 N m^{-2}, while the total interfacial shear stress at the exit of the 1.2 m long condenser was $\sim$0.99 N m^{-2}, but only $\sim$0.52 N m^{-2} at the exit of the same length

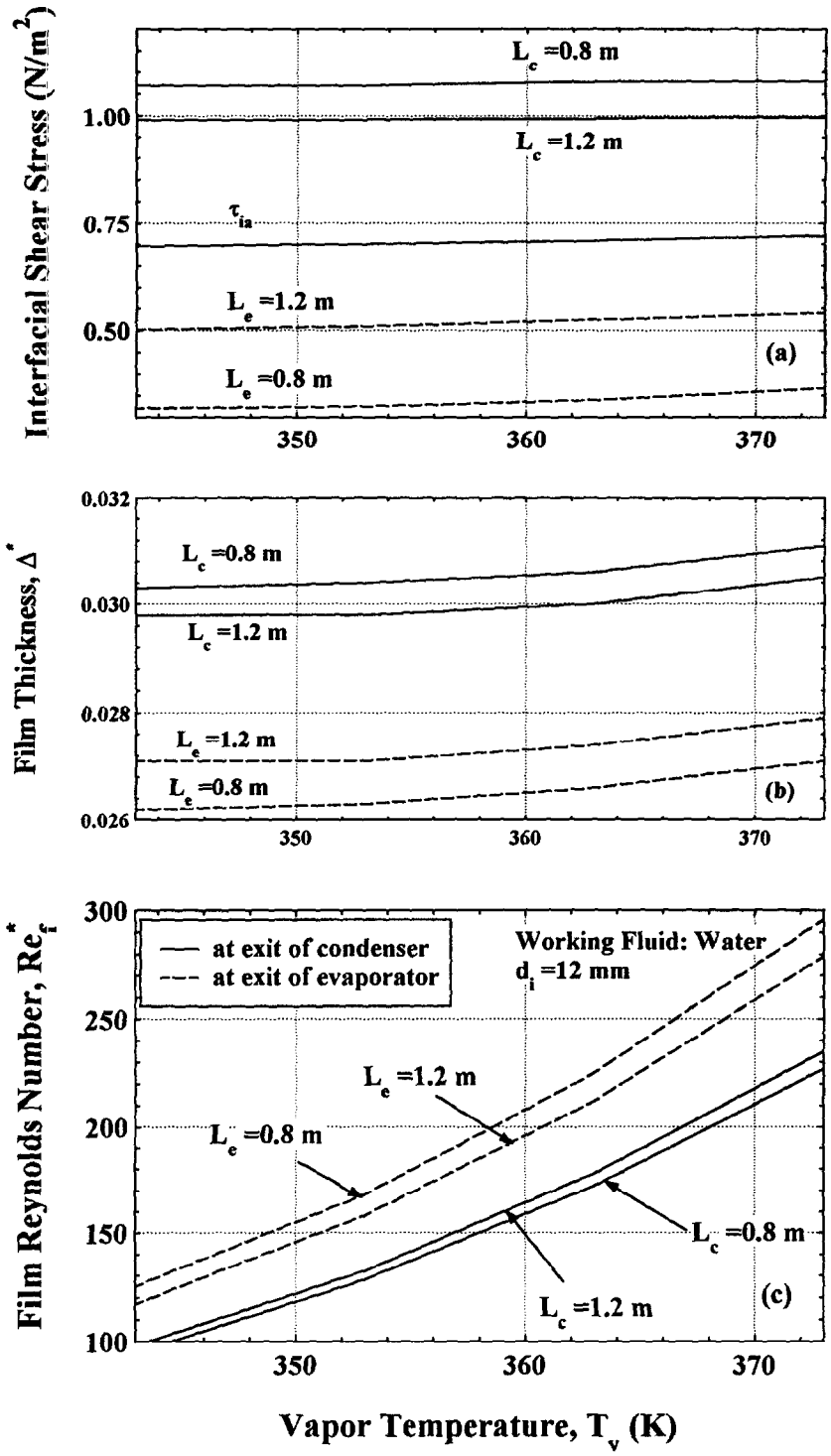

Fig. 3. Comparisons of the values of the liquid film thickness and Reynolds number at CCFL occurring at exit of condenser and evaporator sections.

evaporator section (Fig. 3a). The difference between the adiabatic and the total interfacial shear stress in Fig. 3(a) represents the contribution of the dynamic shear stresses at L–V interface. As Fig. 3 indicates, increasing the condenser length reduced the liquid film thickness, and increased the film Reynolds number for the CCFL at the exit of the condenser. Conversely, increasing the length of the evaporator increased the liquid film thickness, causing CCFL at exit of evaporator to occur at a lower film Reynolds number.

The following analysis focused on assessing the effects of various design and operation conditions for

CCFL at exit of evaporator, since it directly impacts the liquid flow to the evaporator section, and hence liquid film dryout. The values of the film Reynolds number at CCFL at exit of evaporator were compared with experimental data for water and methanol, at different vapor or wall temperatures, and with predictions of other models and the empirical correlation of Faghri *et al.* [8]. Reynolds number values at this CCFL, with and without accounting for the dynamic shear stress at the L–V interface, were also compared to quantify the effect on the model predictions of the conditions for the CCFL.

Figure 4 compares the calculated curves of the power throughput, Q, vs the liquid film thickness at the exit of the evaporator, δ, for methanol, water and R-113 with those predicted by the model of Roesler and Groll [12]; the maxima marked by solid circles indicate the CCFL at the exit of the evaporator. The present model predicts CCFL at the same or a larger film thickness, but consistently at a higher power throughput (or higher film Reynolds number) than Roesler and Groll's [12], owing to the fact that the liquid–vapor interfacial shear stress in the present model is smaller by the effect of the dynamic shear stress. The maximum power throughput also depends on the type of the working fluid; it increases as the vapor pressure of the working fluid decreased, at the same vapor temperature. At a vapor temperature of 303 K, although the calculated water liquid film thickness at CCFL by the present model was about 10% smaller for water than for methanol, the maximum power throughput for water was ~15% higher. At $T_v = 283$ K, the liquid film thickness at CCFL for R113 was about 8% larger, but the maximum power throughput was 70% lower than for methanol.

Comparison with experimental results

Figure 5 compares the calculated liquid film thickness as a function of the film Reynolds number for methanol at wall temperatures of 307, 309 and 311 K. The maximum film Reynolds number indicates CCFL, beyond which the film Reynolds number decreased while the film thickness continued to increase. The results of the present model were also compared with those of the model and experimental data of Reed and Tien for methanol at a wall temperature of 309 K [10]. This temperature was used in the present model to determine the corresponding vapor temperature using equation (34). At low liquid film Reynolds numbers (<30), the predictions of the present model and of Reed and Tien's were in excellent agreement with the experimental data [10] as well as with the Nusselt theory, since the interfacial shear stress is negligible. At higher Reynolds numbers, however, Nusselt theory deviated from the data as the interfacial shear stress at L–V became important, increasing the film thickness in the adiabatic section. As indicated in Fig. 5, the present model was in good agreement with the data, including the values of Reynolds number and the dimensionless film thickness at CCFL (~125 and 0.028, respectively). Reed and Tien's model [10] predicted higher Reynolds number and film thickness (~145 and 0.0335) than their data for the CCFL. These higher values resulted from over estimating the L–V interfacial stress due to neglecting the contribution of the dynamic shear stress. Figure 5 also delineates the effect of changing the wall temperature, while holding the power throughput (or input power) constant. Increasing the wall temperature decreased both the viscosity of the liquid in the film and the liquid flow velocity, hence lowering the L–V interfacial shear stress. Such low interfacial shear stress at high wall temperatures caused the CCFL to occur at higher film Reynolds number and slightly higher film thickness.

Figure 6(a) compares the experimental values of Re_f^* for methanol with the models of Roesler and Groll [12] and Reed and Tien [10] and of the present model. The predictions of Roesler and Groll's model were consistently lower than the data, while those of Reed and Tien's and of the present model were in good agreement with data. It is worth noting, however, that the present model's values of the film Reynolds number at CCFL were lower than Reed and Tien's for $Re_f < 320$, but were slightly higher as at higher Reynolds numbers; note that for a given vapor temperature, the spread in the experimental values of Re_f^* was ~10–15%.

Similar comparisons with the water data of Nguyen-Chi and Groll [18] are shown in Fig. 6(b). The Re_f^* predictions of the present model were in agreement with the data, while those of Reed and Tien model were considerably lower than the data and slightly lower than the present model at low temperatures, but in agreement with data at high temperatures (or high input power). As for methanol (Fig. 6a), the predictions of Roesler and Groll's model for water were consistently lower than the experimental data, and the difference increased as the vapor temperature, or the power throughput, increased. In Fig. 7(a), Re_f^* values of Prenger [7] for methanol were compared with the predictions of the models of Reed and Tien and Roesler and Groll as well as of the present model. The predictions of Reed and Tien's model were about 10% higher than the data, over the whole range of vapor temperatures in the experiments. The predictions of the present model were also in good agreement with the data in the laminar and turbulent film flow regimes. Roesler and Groll's model was slightly lower than the data at low Reynolds number, but considerably lower than the data at higher Reynolds number, both in the laminar and turbulent film flow regimes; Roesler and Groll is not applicable to turbulent liquid film flow. All models, excluding the present model and the empirical correlation of Faghri *et al.* [8], were in good agreement with the data for water (Fig. 6b) at high Reynolds numbers ($Re_f^* > 130$), but lower than the data by about 10–15% at lower Reynolds numbers. The predictions of the present model were in good agreement with exper-

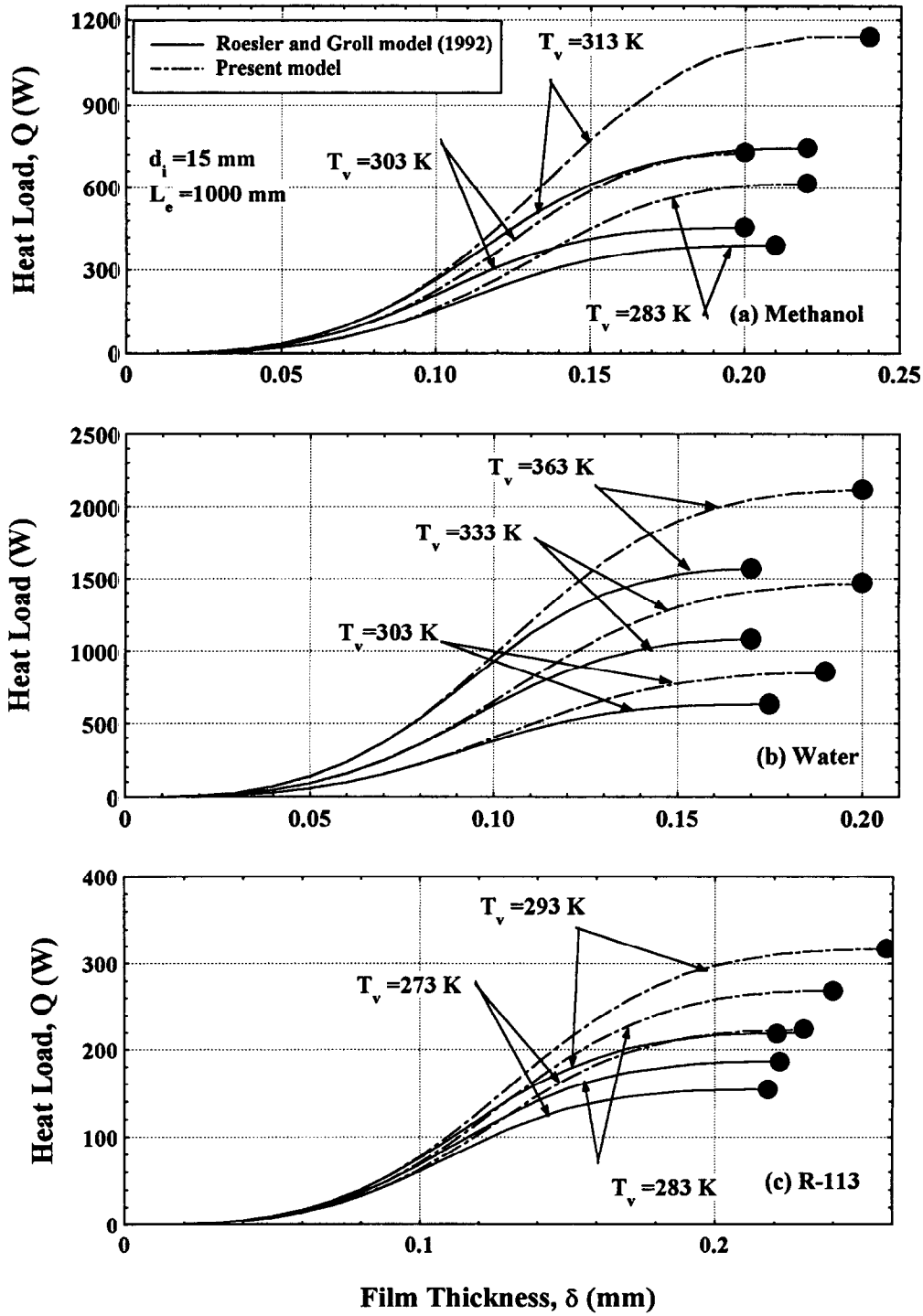

Fig. 4. Comparison of predictions of the present and Roesler and Groll's [12] models of the CCFL at exit of evaporator for methanol, water and R-113.

imental data of water and methanol over the entire range of Reynolds number, to within ±10% (Fig. 7b).

Effect of dynamic shear stress

Figures 6(a) and 8 compared the methanol data of Reed and Tien (1987) with the predictions of the pre-

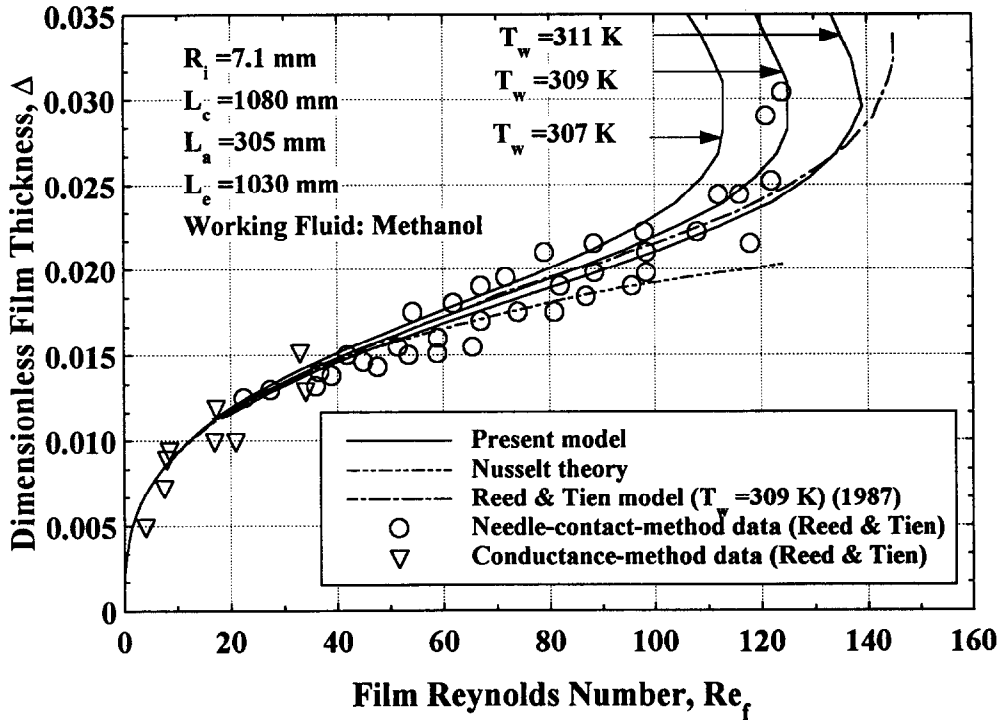

Fig. 5. Comparison of present and Reed and Tien's model with methanol data [10] for the CCFL at exit of evaporator.

sent model, with and without accounting for the dynamic shear stress at the L–V interface. Figure 8 shows that at low Reynolds numbers ($Re_f < 30$), the effect of shear stress at L–V interface was insignificant and the film Reynolds number data was accurately predicted by Nusselt theory. As the film Reynolds number increased the effects of both the adiabatic and dynamic shear stresses at the L–V interface became increasingly important. When only the adiabatic shear stress was considered (solid curve in Fig. 8) the CCFL was predicted at a significantly lower film Reynolds number and higher film thickness ($Re_f^* = 100$ and $\Delta = 0.315$) than the data. When the dynamic shear stress was included, however, the predictions of the present model were in good agreement with the data. For example, in the case of methanol at $T_w = 309$ K, neglecting the dynamic shear stress underestimated Re_f^* by about 22% and over estimated the corresponding film thickness by about 8%. Figure 7(a) also shows that neglecting the dynamic shear stress at L–V interface overpredicted Re_f^* by as much as 50%. Similarly, the water results in Fig. 6(b) indicated that neglecting the dynamic shear stress underpredicted the film Reynolds number at CCFL by about 20–22%.

In the following section, the present model was used to develop operation maps for the film Reynolds number at the CCFL for a number of thermosyphon's working fluids of interest in energy and aerospace applications, namely: R-113, acetone, methanol, heptane, water and Dowtherm-A, for vapor temperature from 250 to 700 K.

CCFL operation maps

For all working fluids considered, the values of Re_f^* were quite sensitive to changes in vapor temperature (Fig. 9). For water, methanol and acetone, Re_f^* values were significantly sensitive to changes in vapor temperature >450, 400 and 390 K, respectively, than at lower temperatures. The useful range of vapor temperature for Dowtherm-A extends from about 520–700 K, while that for water extends from ~300 to 490 K. For Dowtherm-A, the film Reynolds number at CCFL increases with increased vapor temperature, but at a lower rate than other working fluids. Figures 9(a, b) indicate that increasing the inner diameter of a thermosyphon increased not only the Reynolds number at CCFL, but also the rate of change in the film Reynolds number with increased vapor temperature. For example, at a vapor temperature of 600 K, the Reynolds number at the CCFL for Dowtherm-A more than doubled, from 1796 to 3726, as the thermosyphon inner diameter increased from 15 to 28 mm. Similarly, at a water vapor temperature of 460 K, increasing the thermosyphon inner diameter from 15 to 28 mm increased Reynolds number at CCFL for water from 1949 to 4299.

Figure 10 presents the calculated values of the film Reynolds number at CCFL as well as the cor-

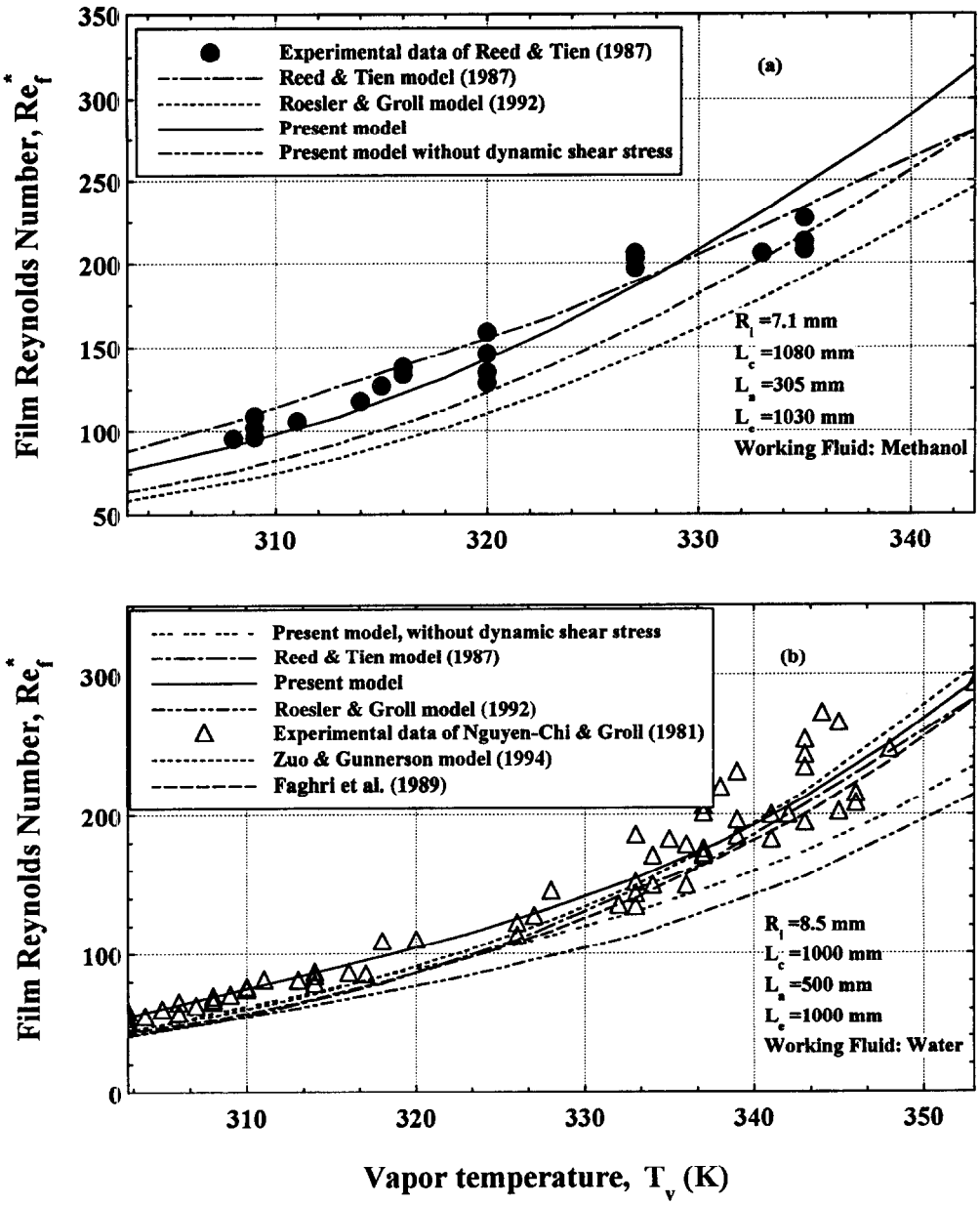

Fig. 6. Comparison of CCFL predictions with methanol [10] and water data [18] for the CCFL at exit of evaporator.

responding maximum power throughput, as functions of the vapor temperature for heptane, acetone and Dowtherm-A. The film Reynolds numbers at CCFL (or the maximum power throughput) for heptane and acetone increased slowly with increased vapor temperature up to 330 and 390 K, respectively, then increased rapidly with further increase in the vapor temperature. For Dowtherm-A, however, the maximum power throughput increased initially precipitously with increased vapor temperature up to 540 K, then slowly with a further increase in the vapor temperature. Because of the differences in the physical properties and vapor pressures of the different working fluids, at the same vapor temperature the values of the maximum power throughput (or film Reynolds number at CCFL) were different (Fig. 10). For example, at a vapor temperature of 350 K, the maximum power throughput for heptane and acetone was 595 and 1110 W, respectively. For Dowtherm-A, which has a significantly lower vapor pressure, a temperature of 350 K was outside its operating range of ~520–690 K. For this operating temperature range, the maximum power throughput varied from 300 to 1075 W. For heptane a maximum power throughput of 300 W corresponds to a vapor temperature of 289 K. This temperature, however, was outside the operating

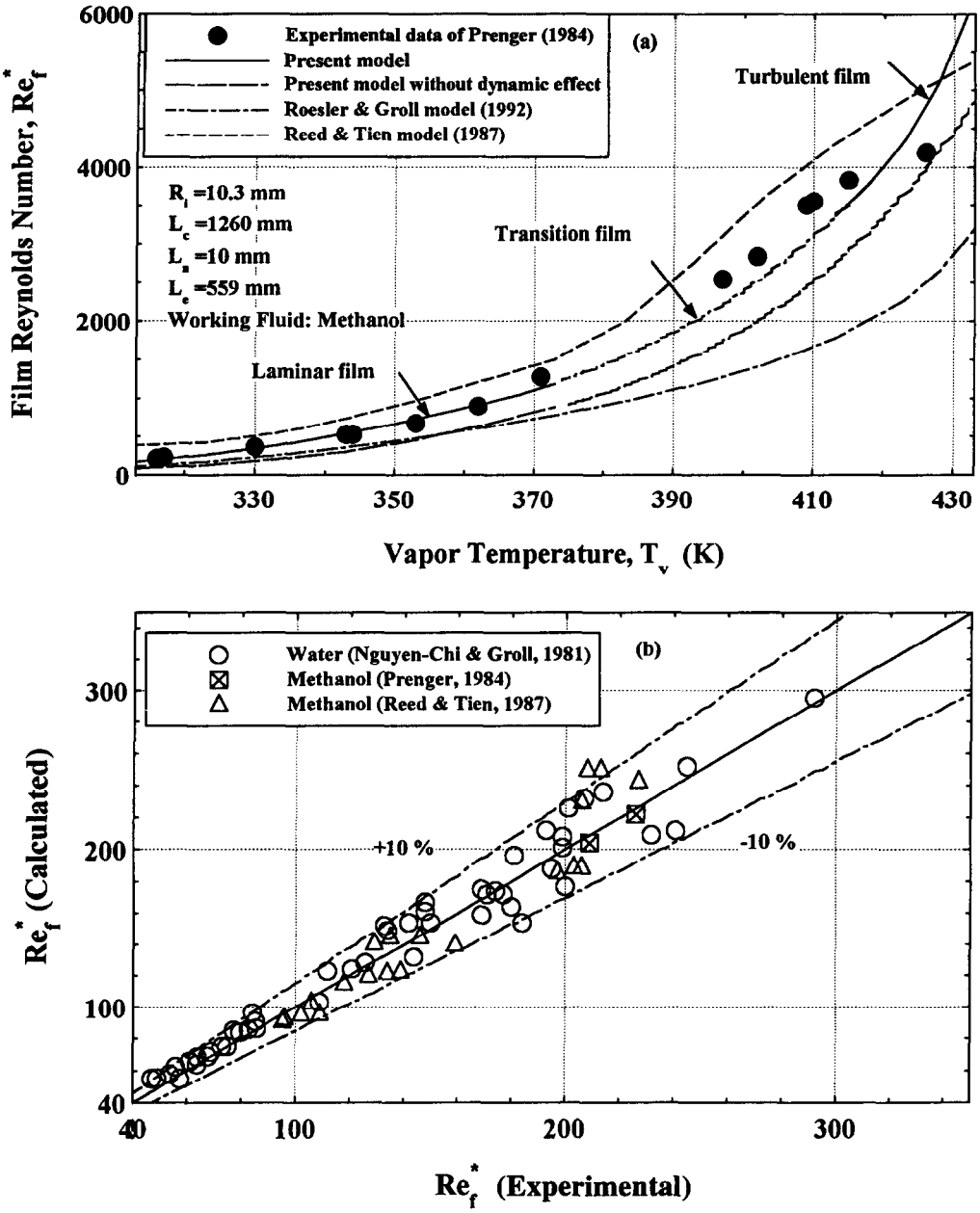

Fig. 7. Comparison of the model predictions with methanol [7, 10] and water data [18] for CCFL at exit of evaporator.

range of acetone (Fig. 10). On the other hand, a power throughput of 1075 W for acetone corresponds to a vapor temperature of 347 K, which was outside the operating range of heptane.

In summary, the CCFL maps delineated in Fig. 9(a, b), could be an effective design tool for selecting the appropriate working fluid for the operating temperature range from 250 to 700 K. In general, the lower the vapor pressure of the working fluid the higher was the maximum operating vapor temperature. For a given vapor temperature, the Reynolds number at the CCFL increased with increased vapor pressure of the working fluid. Increasing the inner diameter of a thermosyphon has also been shown to significantly increase the values of the film Reynolds number at the CCFL (more details are given in the next section). It is worth noting, however, that the chemical compatibility of the working fluid with the wall material of the thermosyphon would impact the final choice of the working fluid for a given application.

Effect of thermosyphon diameter

Figure 11 examined the effect of the thermosyphon inner diameter on the film Reynolds number at CCFL for R-113, methanol and water. Increasing either the

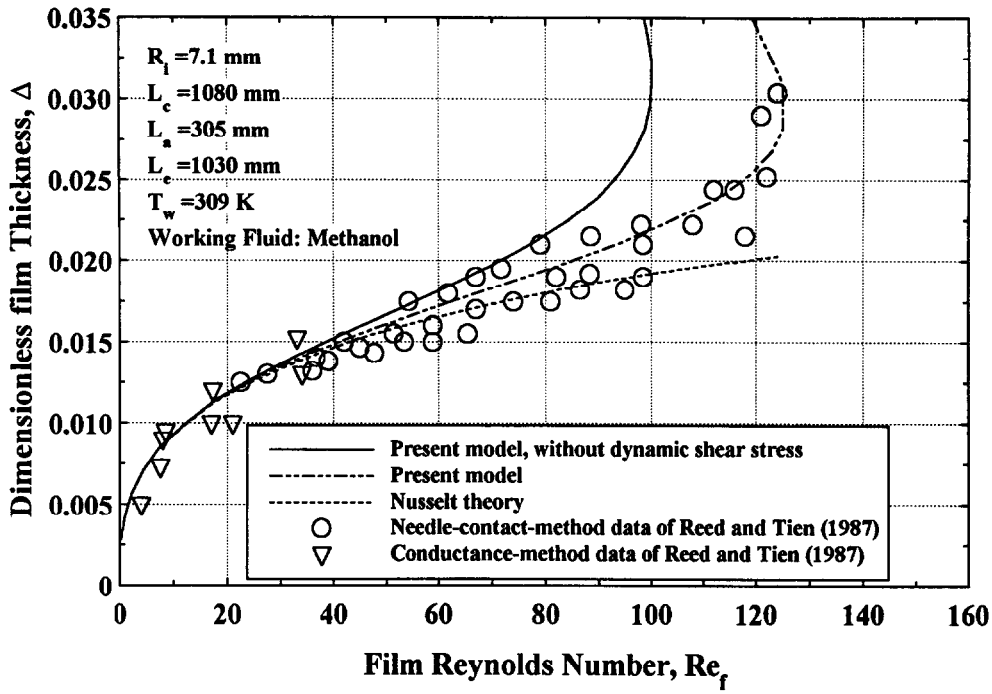

Fig. 8. Effect of the dynamic shear stress on the values of the liquid film Reynolds number and thickness for CCFL of methanol [10] at exit of evaporator.

thermosyphon's inner diameter or the vapor temperature increased Reynolds number at CCFL. For a given power throughput or film Reynolds number, increasing the inner diameter of a thermosyphon, however, increased the vapor flow area, hence lowering the vapor flow velocity and the evaporation mass flux at the L–V interface. While the low vapor velocity decreased the interfacial shear stress at the L–V interface, the low evaporation mass flux decreases the dynamic shear stress due to evaporation, which increased the total interfacial shear stress (the total interfacial shear stress is equal to the adiabatic shear stress minus the dynamic shear stress due to evaporation at L–V interface [15, 16]). Because the effect of the former outweighs the latter, the total shear stress at the L–V interface effectively decreased as the inner diameter of the thermosyphon increases. Such low interfacial shear stress caused the CCFL for the large diameter thermosyphon to occur at both higher Reynolds number (or higher power throughput) and higher liquid film thickness and, hence, higher interfacial shear stress (Fig. 11(a, b)).

Similarly, for a given power throughput or film Reynolds number, increasing the vapor temperature decreased the vapor velocity (due to higher vapor density), the liquid viscosity and latent heat of vaporization. The latter increased the evaporation mass flux, increasing the dynamic shear stress due to evaporation and, hence, decreased the total shear stress at the L–V interface. The low vapor velocity also decreased the interfacial shear stress and the low liquid viscosity decreased the adiabatic shear stress. The net result was a decrease in the total shear stress at the L–V interface, causing CCFL to occur at both higher Reynolds number and higher liquid film thickness. Figure 11(a, b) indicates that for a given vapor temperature, increasing the diameter of a thermosyphon significantly enhanced its performance by increasing the value of the film Reynolds number at CCFL (or the maximum power throughput).

Effect of evaporator length

Figure 12 shows the results on the effect of the evaporator length on the values of the liquid film Reynolds number and dimensionless thickness at the CCFL. For a given vapor temperature and a thermosyphon inner diameter, increasing the evaporator section length appreciably decreased the film Reynolds number at CCFL, for short and intermediate evaporator lengths ($Le < 1000$ mm), but only slightly for longer evaporator sections. For the same power throughput, while increasing the evaporator length did not change the vapor velocity at the exit of the evaporator, it lowered the evaporation mass flux at the L–V interface, and hence the dynamic shear stress. The low dynamic shear stress resulted in a higher total interfacial shear stress at L–V interface and a higher liquid film thickness at the CCFL (Fig. 12b). Conversely, the large increase in the total interfacial shear with increased evaporator length caused the CCFL to occur at lower film Reynolds number, or lower maximum power throughput (Fig. 12a).

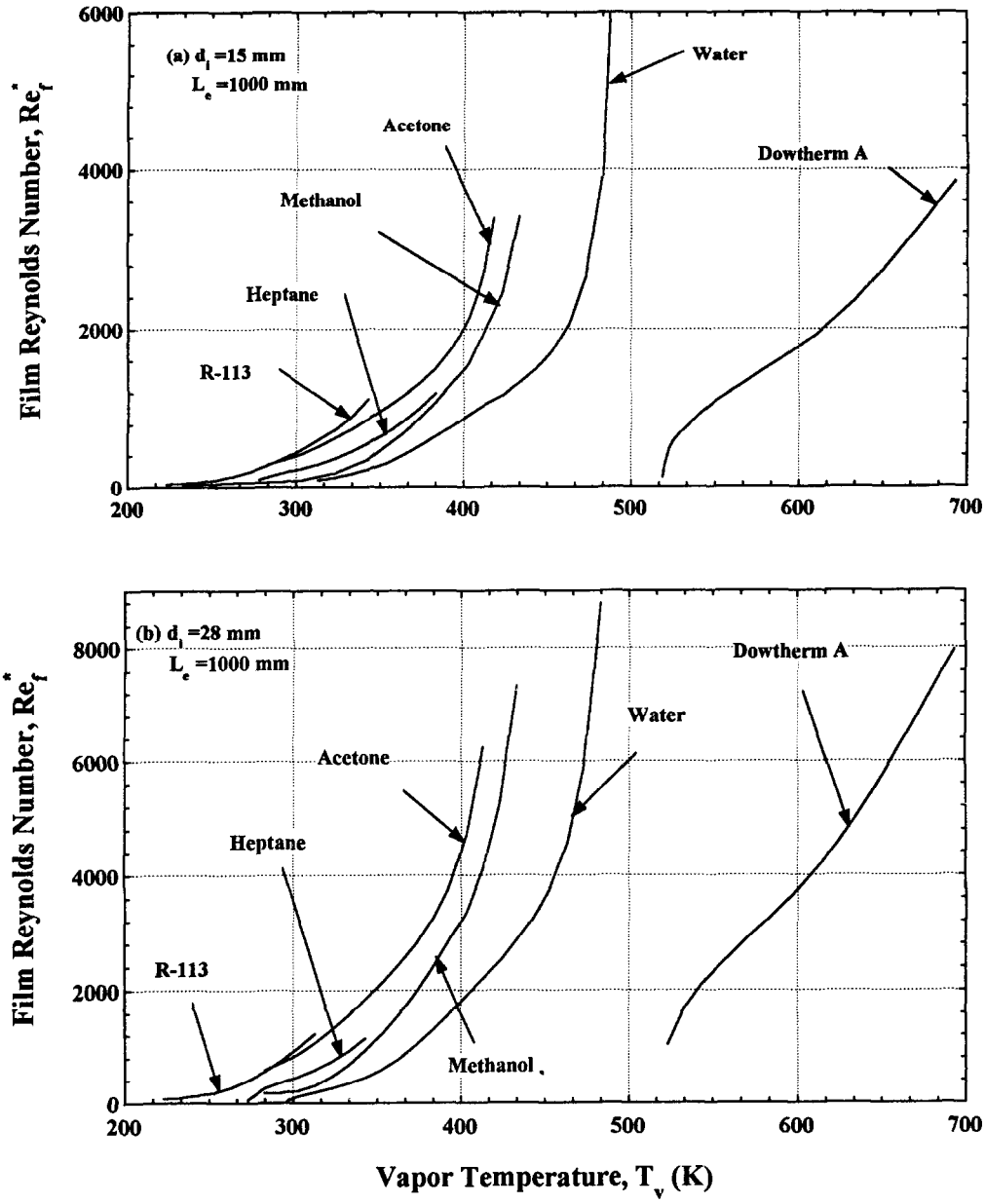

Fig. 9. Film Reynolds numbers for CCFL of different working fluids at exit of evaporator.

SUMMARY AND CONCLUSIONS

An analytical model was developed to predict CCFL in GATPTs, which incorporated the shear stress at the L–V interface as the sum of: (a) the adiabatic shear stress, calculated using available correlations; and (b) the dynamic shear stress, which accounts for the effect of evaporation at the interface. The model predictions of the film Reynolds number at the CCFL were consistently in good agreement with both the laminar and turbulent liquid film data of other investigators for methanol and water, to within $\pm 10\%$. This good agreement, considering the uncertainties and the spread in the reported experimental data, supports the current approach for determining the shear stress at the L–V interface in GATPTs.

The results indicated that at low Reynolds numbers the effect of interfacial shear stress was insignificant and the liquid film Reynolds number can be accurately calculated using the Nusselt solution. At intermediate and high liquid film Reynolds numbers, however, the shear stress at the L–V interface became important, including the dynamic component. Neglecting the contribution of the dynamic shear stress underpredicted the film Reynolds number at CCFL as much as 22% for methanol and 20% for water. The cor-

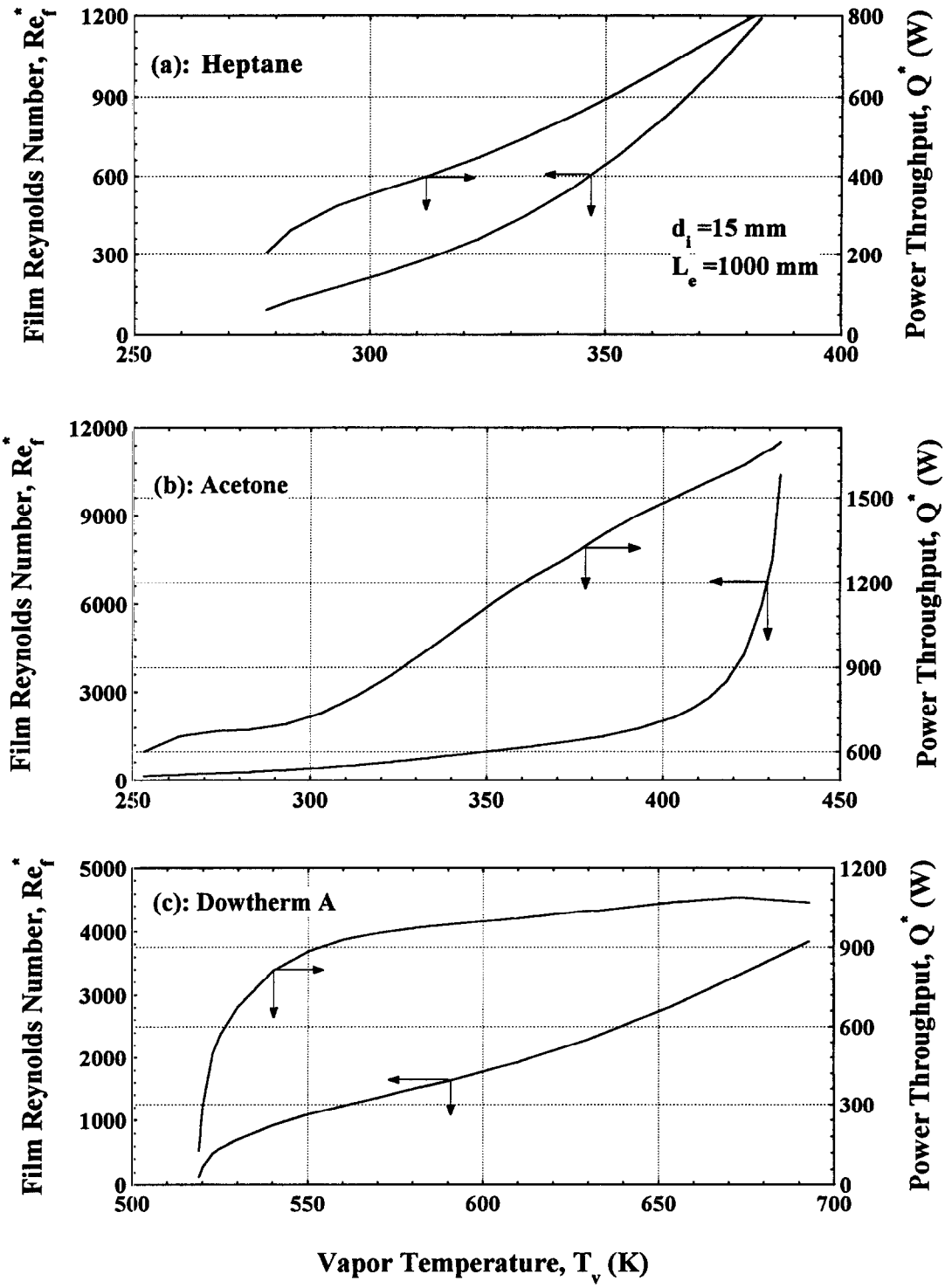

Fig. 10. Film Reynolds number and maximum power throughput corresponding to CCFL for heptane, acetone and Dowtherm-A at exit of evaporator.

responding film thicknesses in the adiabatic section for both methanol and water were overpredicted, but by smaller percentages.

Operation maps for a number of working fluids of interest in aerospace and energy applications, namely: R-113, acetone, methanol, heptane, water and Dowtherm-A were developed and discussed. These maps give the film Reynolds number (or the maximum

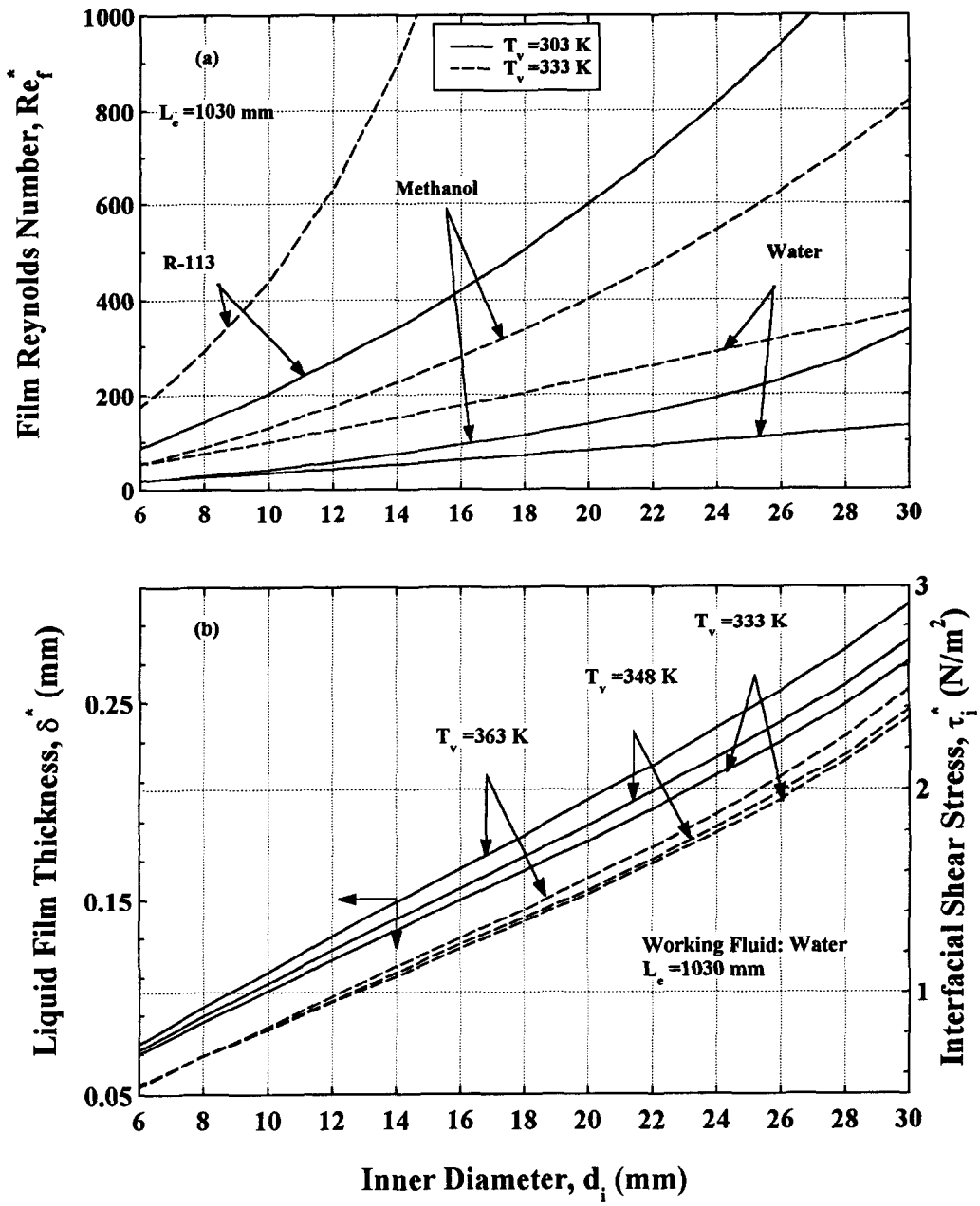

Fig. 11. Effect of thermosyphon inner diameter on film Reynolds number and thickness and interfacial shear stress for CCFL at exit of evaporator.

power throughput) at CCFL as a function of vapor temperature from 250 to 700 K. The useful range of vapor temperatures for Dowtherm-A extended from 520 to 700 K, while that for water, which has a higher vapor pressure, extended only from 300 to 490 K. Despite the smaller operating range for water, the corresponding values of Reynolds number at CCFL of 83–6314 (or maximum heat load of 1698–8503 W), for a thermosyphon having a diameter of 15 mm and an evaporator length of 1000 mm, were much higher than those for Dowtherm-A of 279–4015 (or maximum heat load of 289–1048 W).

The values of Re_f^* (or of the maximum power throughput) significantly increased as the inner diameter of the thermosyphon increased, and to much lesser extent, as the length of the evaporator section decreased. The results also showed that increasing either the vapor temperature or the thermosyphon inner diameter increased the value of Reynolds number at the CCFL. Conversely, increasing the evaporator length decreased the value of Reynolds number at CCFL for small and intermediate evaporator lengths (< 1000 mm); for longer evaporators, however, the decrease in the value of Reynolds number at

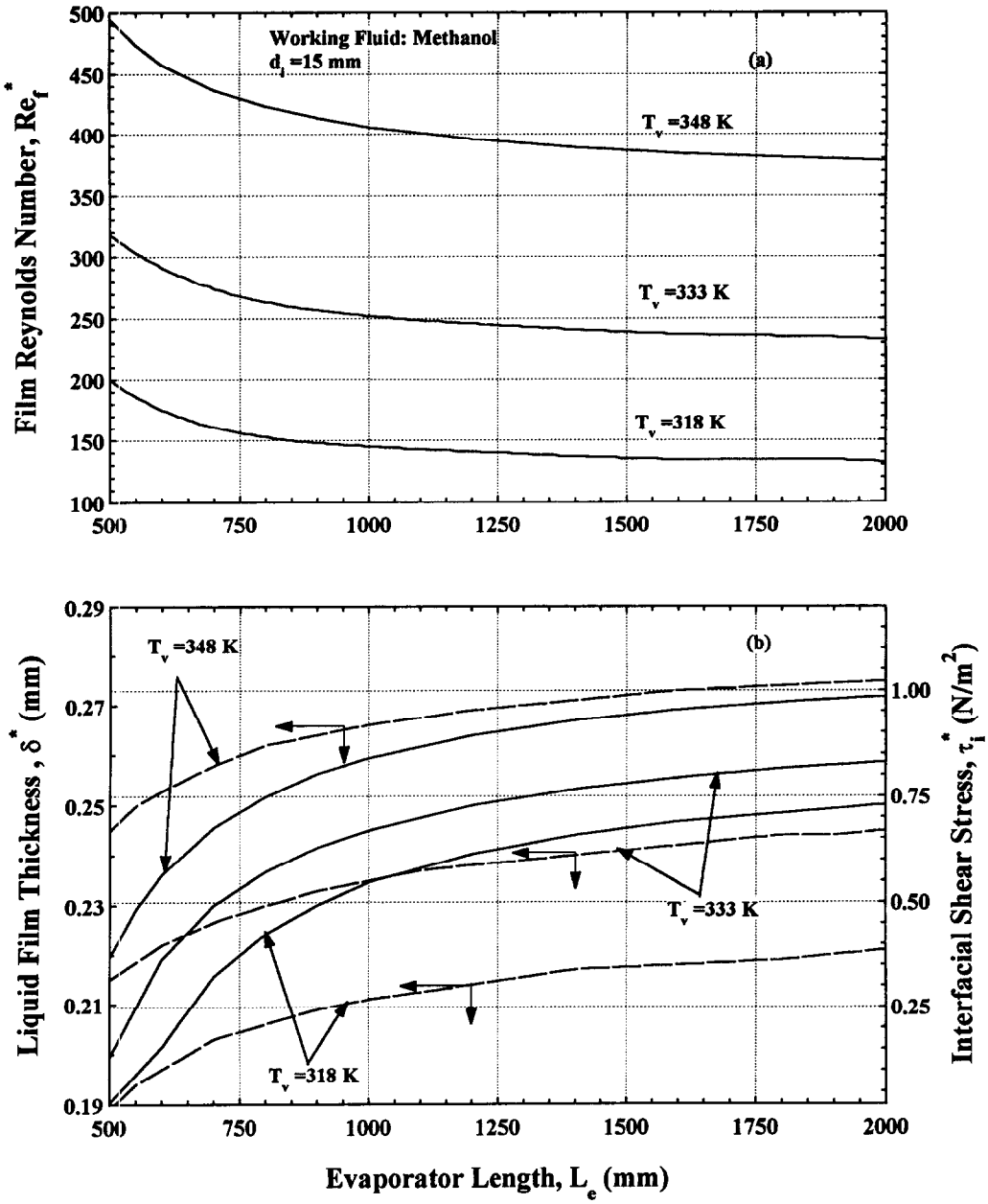

Fig. 12. Effect of evaporator length on film Reynolds number and thickness and interfacial shear stress for CCFL at exit of evaporator.

CCFL with increased evaporator length was significantly smaller.

Acknowledgments—This research is partially funded by the University of New Mexico's Institute for Space Nuclear Power studies and the Egyptian Authority for Scientific Missions, Cairo, Arab Republic of Egypt.

REFERENCES

1. Shiraishi, M., Yoneya, M. and Yabe, A., Visual study of operating limit in the two-phase closed thermosyphon, *Proceedings of the 5th International Heat Pipe Conference*, 1984, pp. 10–17.
2. Bharathan, D., Wallis, G. B. and Richter, H. J., *Air-Water Countercurrent Annular Flow*. EPRI Report no. EPRI NP-1165, 1979.
3. Wallis, G. B., *One-Dimensional Two-Phase Flow*. McGraw-Hill, New York, 1969.
4. Tien, C. L. and Chung, K. S., Entrainment limits in heat pipes. *Proceedings of the 3rd International Heat Pipe Conference*, Palo Alto, CA, 1978, pp. 36–40.
5. Bezrodnyi, M. K., The upper limit of maximum heat transfer capacity of evaporative thermosyphons. *Teploenergetika*, 1978, **25**, 63–66.
6. Imura, H., Sasaguchi, K. and Kozai, H., Critical heat flux in closed two-phase thermosyphons. *International Journal of Heat and Mass Transfer*, 1983, **26**(8), 1181–1188.

7. Prenger, F. C., Performance limits of gravity-assisted heat pipes. *Proceedings of the 5th International Heat Pipe Conference*, 1984, Part 1, pp. 1–5.
8. Faghri, A., Chen, M. M. and Morgan, M., Heat transfer characteristics in two-phase closed conventional and concentric annular thermosyphons. *Journal of Heat Transfer*, 1989, **111**, 611–618.
9. Dobran, F., Steady-state characteristics and stability thresholds of a two-phase thermosyphon. *International Journal of Heat and Mass Transfer*, 1985, **28**, 949–957.
10. Reed, J. G. and Tien, C. L., Modeling of the two-phase closed thermosyphon. *Journal of Heat Transfer*, 1987, **109**, 722–730.
11. Zuo, Z. J. and Gunnerson, F. S., Numerical study of the thermosyphon flooding limit. *Fundamentals of Heat Pipes*, ASME HTD, 1994, **278**.
12. Roesler, S. and Groll, M., Flow visualization and analytical modeling of interaction phenomena in closed two-phase flow systems. *Proceedings of the 8th International Heat Pipe Conference*, Beijing, China, Institute of Engineering Thermophysics, Chinese Academy of Sciences, 1992, pp. 26–32.
13. Peterson, G. P. and Bage, B. K., Entrainment limitations in thermosyphons and heat pipes. *Journal of Energy Resources Technology*, 1991, **113**, 147–153.
14. Grolmes, M. A., Lambert, G. A. and Fauske, H. K., Flooding in vertical tubes. *AIChE Symposium Series No. 38, Multiphase Flow Systems*, Paper no. A4, 1974.
15. Linehan, J. H., The interaction of two-dimensional stratified, turbulent air–water and steam–water flows. Ph.D. dissertation, University of Wisconsin, 1968.
16. Lee, S. C. and Bankoff, S. G., Stability of steam–water countercurrent flow in an inclined channel: flooding. *Journal of Heat Transfer*, 1983, **105**, 713–718.
17. Collier, J. G., *Convective Boiling and Condensation*, 2nd edn. McGraw-Hill, New York, 1981, Chapter 10, pp. 314–359.
18. Nguyen-Chi, H. and Groll, M., Entrainment for flooding limit in a closed two-phase thermosyphon. In *Advances in Heat Pipe Technology*, ed. D. A. Reay. Pergamon Press, New York, 1981, pp. 147–162.